Chinese Chemical Letters 34 (2023) 108305

Contents lists available at ScienceDirect

Chinese Chemical Letters

journal homepage: www.elsevier.com/locate/cclet

# Tungsten oxide nanowires and polyaniline hybrid film-based electrochromic device with multicolor display and enhanced capacitance

Yanan Chen[a,1], Jiao Lei[a,1], Yanling Zhai[a,*], Zhijun Zhu[b,*], Weitai Wu[c], Xiaoquan Lu[a,*]

[a] Institute of Molecular Metrology, College of Chemistry and Chemical Engineering, Qingdao University, Qingdao 266071, China
[b] Institute of Hybrid Materials, National Center of International Research for Hybrid Materials Technology, National Base of International Science & Technology Cooperation, College of Materials Science and Engineering, Qingdao University, Qingdao 266071, China
[c] State Key Laboratory of Physical Chemistry of Solid Surfaces, Xiamen University, Xiamen 361005, China

ARTICLE INFO

*Article history:*
Received 25 October 2022
Revised 6 February 2023
Accepted 5 March 2023
Available online 12 March 2023

*Keywords:*
$W_{18}O_{49}$/PANI
Electrochromism
Multifunctional devices
Multicolor
Energy storage

ABSTRACT

Electrochromic devices (ECDs) have exhibited promising applications in the fields of energy-saving intelligent buildings and next-generation displays because of their simple structure, low power consumption, and multicolor displays. $W_{18}O_{49}$/polyaniline (PANI) hybrid films are prepared and assembled to ECDs. Compared with pure PANI and $W_{18}O_{49}$ films, the hybrid film exhibits superior electrochemical and electrochromic performance, including high optical modulation (70.2%), large areal capacity (79.6 mF/cm$^2$), and good capacitance retention. The excellent electrochemical and electrochromic performance is ascribed to the formation of the donor (PANI)-acceptor ($W_{18}O_{49}$) pair, the porous structure in the nanowires, and the large surface area, which enhance electron delocalization of the $W_{18}O_{49}$/PANI, improve the ion diffusion rate, and increase the charge storage sites. Furthermore, benefitting from the outstanding optical, electrical, and multifunctional properties, the $W_{18}O_{49}$/PANI hybrid film-based ECD platform is expected to play an important role in electrochromism and energy storage.



With the increasing energy demand and environmental pollution, more and more attention has been paid to the green economy, so the issue of efficient energy storage and energy conservation has gradually become the primary concern [1–3]. In recent years, ECD with bifunctional properties of electrochromism and energy storage has been developed as an excellent technology to meet the above requirements for a green world [4,5]. ECDs can achieve reversible color changes and dynamic regulation of light transmission, absorption, and reflectivity through low voltage control (usually <4 V) [6–9], which have broad application prospects in smart windows, static displays, automotive anti-glare rearview mirrors, electronic paper, and energy storage fields [10,11].

Moreover, the development of electrochromic materials in energy storage devices has attracted widespread attention [12–14]. The most studied electrochromic materials mainly include transition metal oxides (*e.g.*, $WO_3$, NiO, $V_2O_5$, and $Nb_2O_5$), Prussian blue [15–19], and organic materials such as viologen compounds, PANI, polypyrrole [20,21]. For example, Prussian blue film incorporated with an aluminum (Al) electrode integrated bi-functional electrochromic and energy storage ability into one device [22]. Nevertheless, monotonous color change, slow switching speed, and low capacity greatly limit the application of devices constructed from one electrochromic material. The ECDs with inorganic/organic hybrid films that combine the advantages of conducting conjugated polymers and transition oxides have gained much recent research interest. For instance, Cai and co-workers reported $TiO_2$/PANI nanocomposites displayed remarkable improvement in transmittance modulation and cycling stability compared with PANI film [23]. Similarly, Shi *et al.* developed $WO_3$/poly(3,4-ethylenedioxythiophene) (PEDOT) core@shell hybrid nanorod arrays, which exhibited promising electrochromic performance of much shorter switching time and enhanced optical contrast because of a synergistic effect between the $WO_3$ nanocore and the PEDOT nanoshell [24]. However, the wide application of these devices is limited by their inadequate energy storage capacity. Hence, developing a novel hybrid film-based ECD with excellent electrochromic properties and high capacitance is of great significance, which provides a valuable technical application direction for the next generation of smart windows and power supply.

* Corresponding authors.
*E-mail addresses:* zhaiyanling@qdu.edu.cn (Y. Zhai), zhuzhijun@qdu.edu.cn (Z. Zhu), luxq@nwnu.edu.cn (X. Lu).
[1] These authors contributed equally to this work.

https://doi.org/10.1016/j.cclet.2023.108305
1001-8417/

It is well known that $WO_{3-x}$ as a typical cathodic material has excellent properties of high cycle stability [25,26], and good optical contrast, but it has the disadvantages of monotonous color and long switching time. As an anodic electrochromic material, PANI has the advantages of adjustable electrical conductivity and multicolor switching but always possesses poor durability [27,28]. The hybrid material of $WO_{3-x}$ and PANI is expected to give full play to the advantages of the two materials, which would work as electrochromic devices with higher stability and a multicolor display [29]. More importantly, both $WO_{3-x}$ and PANI are suitable electrode materials to construct electrochromic energy storage devices [15,30], because of their pseudocapacitive properties [16,20,31,32].

Herein, $W_{18}O_{49}$/PANI hybrid film is constructed through the electropolymerization of the PANI layer on solvothermal synthesized $W_{18}O_{49}$ film. Compared with the pure PANI film, the hybrid film exhibits richer color, a wide optical modulation range, improve switching speed, and excellent durability. Moreover, the incorporation of the $W_{18}O_{49}$ for hybrid film leads to remarkable improvements in energy storage capacity, which is mainly attributed to the synergistic effect between $W_{18}O_{49}$ and PANI, the porous space of the $W_{18}O_{49}$/PANI boosting the fast ion diffusion and providing the charge-transfer reactions with large surface area. The as-synthesized $W_{18}O_{49}$/PANI hybrid film shows great potential in electrochromic and energy storage applications.

The fabrication of $W_{18}O_{49}$/PANI film involves a two-step process (Fig. 1a). First, $W_{18}O_{49}$ nanowires were synthesized on fluorine-doped $SnO_2$ (FTO) glass substrate by solvothermal method. Secondly, the $W_{18}O_{49}$ was coated by the PANI through an electrochemical deposition of aniline. Field emission scanning electron microscope (FE-SEM) image reveals that the $W_{18}O_{49}$ nanowires (Fig. S1 in Supporting information) are of an average length of several micrometers and a width of 10–20 nm in Fig. 1b, which provides a porous spatial structure for ion transport. The inset shows the microscopy picture of the synthesized $W_{18}O_{49}$ film (Fig. S1), which is nearly transparent. After the electrochemical polymerization of PANI on the surface of the $W_{18}O_{49}$ film, a green PANI layer [31] made of short rod cross-linked curd was deposited (Fig. 1c), indicating the successful fabrication of $W_{18}O_{49}$/PANI film. Fig. S2 (Supporting information) shows the FE-SEM images of the FTO substrates before and after electrochemically polymerization of short rod-shaped PANI.

The element distribution images in Fig. S3 (Supporting information) show that W, N, and C are uniformly distributed throughout the film. X-ray diffraction (XRD) patterns in Fig. 1d show the sharp diffraction peaks of $W_{18}O_{49}$ at 23.50°, 26.23°, 35.34°, and 48.00°, confirming the successful preparation of monoclinic $W_{18}O_{49}$ (JCPDS No. 84–1516) [31]. X-ray photoelectron spectroscopy (XPS) is used to study the surface state of film. The peaks at 35.42/37.55 and 33.97/35.95 eV are ascribed to the binding energies of $W^{6+}$ and $W^{5+}$ in $W_{18}O_{49}$ (Fig. S4 in Supporting information), respectively, indicating the mixed valence of W [26]. Moreover, N, O, W, and C can be found in the XPS spectrum of the as-prepared $W_{18}O_{49}$/PANI hybrid film (Fig. S5 in Supporting information), indicating the coexistence of $W_{18}O_{49}$ and PANI. In contrast, no characteristic N 1s peak is observed in the $W_{18}O_{49}$ film (Fig. S6 in Supporting information). As shown in Fig. 1e, the N 1s broad band at 399.57 eV of $W_{18}O_{49}$/PANI film can be deconvoluted into three N species at 398.88, 399.5, and 401.04 eV, [33,34] which are assigned to quinoline phenyl structure (-N=), benzene structure (-NH-), and quaternary ammonium structure ($N^+$) [27,33,35], respectively, and these peaks can also be found in the N 1s XPS spectrum of the PANI film. The similar phenomenon can be observed in the W 4f spectrum of the $W_{18}O_{49}$/PANI film (Fig. S7 in Supporting information). All these results demonstrate the successful synthesis of $W_{18}O_{49}$/PANI hybrid film.

Fig. S8 (Supporting information) shows the current density profiles of the electrodepositing PANI film onto FTO and $W_{18}O_{49}$ substrates. A larger current density on FTO was observed due to the better conductivity of the FTO substrate than $W_{18}O_{49}$. As the thickness of PANI increases, the color change of the $W_{18}O_{49}$/PANI hybrid film is more obvious. As shown in Fig. S10 (Supporting information), when the deposition time was increased to 400 s, no significant improvement in the color change of the hybrid film can be seen. Therefore, a deposition time of 300 s is selected for further study and discussion.

The CV curves of the PANI and the $W_{18}O_{49}$/PANI hybrid films in 1 mol/L $AlCl_3$ aqueous solution between −0.6 V and 1.0 V are presented in Fig. 2a. The hybrid film exhibits good pseudocapacitive behavior [36–38] with two pairs of redox peaks of PANI marked with blue triangles. The two peaks marked with red triangles in Fig. 2a represent the characteristic redox reaction [15,39] of $W_{18}O_{49}$ from −0.1 V to −0.6 V (Fig. S11 in Supporting information), which is only found in the $W_{18}O_{49}$/PANI hybrid film. The redox reaction of $W_{18}O_{49}$/PANI film involves the intercalation and extraction processes of chlorine anion ($Cl^-$) and aluminum ion ($Al^{3+}$)

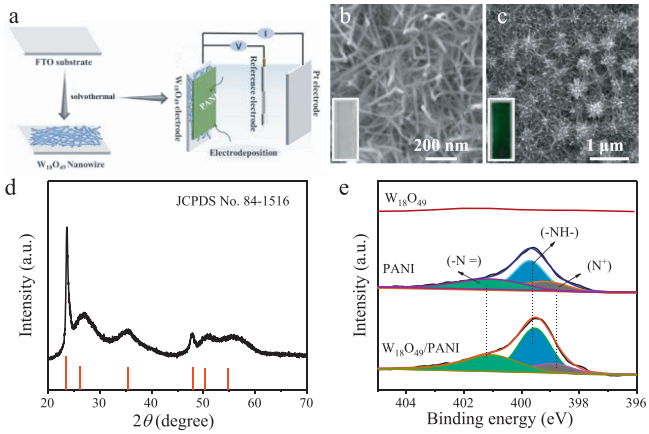


**Fig. 1.** (a) Schematic illustration of the fabrication of the $W_{18}O_{49}$/PANI film. (b, c) SEM image of $W_{18}O_{49}$ and $W_{18}O_{49}$/PANI film (the inset is the photograph of the corresponding film). (d) The XRD pattern of $W_{18}O_{49}$ on the FTO glass. (e) The N 1s XPS of $W_{18}O_{49}$, PANI, and $W_{18}O_{49}$/PANI.

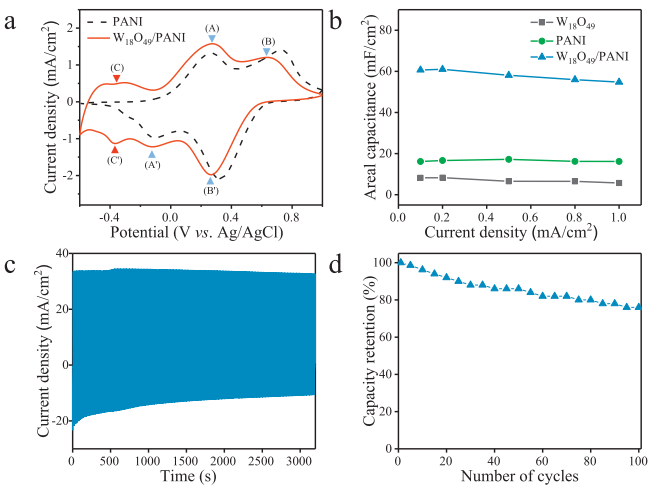


**Fig. 2.** Energy storage performances and cycle stability are characterized by electrochemical measurements. (a) Cyclic voltammetry curves for PANI and $W_{18}O_{49}$/PANI hybrid thin film between −0.6 V and 1.0 V at 40 mV/s in 1 mol/L $AlCl_3$ aqueous solution. (b) The areal capacitance of the three films at different current densities of 1.0, 0.8, 0.5, 0.2, and 0.1 mA/cm$^2$. (c) The chronoamperometry (CA) curves of $W_{18}O_{49}$/PANI hybrid film at the alternant potential of −0.6 V and 1.0 V (*vs.* Ag/AgCl, each for 10 s) in 1 mol/L $AlCl_3$ aqueous solution. (d) The energy storage cycle stability of the $W_{18}O_{49}$/PANI film at a current density of 1.0 mA/cm$^2$.

[21,35,40-42], which is fully explained in Fig. S12a (Supporting information). It means that both $W_{18}O_{49}$ and PANI components in the hybrid film exhibit individual electrochemical activities, and they can simultaneously switch to colored/bleached states under positive/negative voltage applications.

The $W_{18}O_{49}$/PANI hybrid film shows much enhanced exchange current density at around −0.5 and −0.2 V (peak C, C′ in Fig. 2a) than that of PANI film, because of the redox behavior of $W_{18}O_{49}$. Moreover, the relative current density of the hybrid film at −0.3 and 0.3 V (peak A, A′ in Fig. 2a and Fig. S12a) are much higher than that of PANI film (peak A and A′ in Fig. S13a in Supporting information), which further demonstrates the formation of the donor (PANI)-acceptor ($W_{18}O_{49}$) pair. The fine structure can be well maintained in its CV curve even at a scan rate as high as 100 mV/s, demonstrating that a large number of active sites in the hybrid film can be efficiently oxidized/reduced due to the fast charge transfer of $W_{18}O_{49}$ nanowires and the synergistic effect between $W_{18}O_{49}$ nanowires and PANI. The surface of the $W_{18}O_{49}$ nanowires is relatively rough, which provides a large active specific surface area for the electrochemical reaction process. Fig. S12b (Supporting information) shows the relationship between the anodic and cathodic peak current densities of $W_{18}O_{49}$/PANI versus the square root of the scanning rate. An approximately linear relationship can be found, indicating that the entire reaction process is diffusion-controlled.

The capacitive performance is investigated with the galvanostatic charge/discharge (GCD) test. $W_{18}O_{49}$, PANI, and $W_{18}O_{49}$/PANI hybrid electrodes are charged and discharged at different current densities respectively (Fig. S12c in Supporting information). The discharge time of the $W_{18}O_{49}$/PANI film is much longer than that of the individual $W_{18}O_{49}$ and PANI films, indicating the superior capacitance properties of $W_{18}O_{49}$/PANI film, which may be attributed to the synergistic effect between $W_{18}O_{49}$ and PANI. Firstly, the porous structure in the hybrid film provides excess active area, allowing more doped electrons ions to enter the $W_{18}O_{49}$/PANI thus enhancing the charge storage capacity. Secondly, due to the formation of donor-acceptor pair between PANI and $W_{18}O_{49}$, PANI chains could locally donate more electrons to $W_{18}O_{49}$ [24], which further accelerates the electron migration and improve the ion diffusion efficiency.

The areal-specific capacitance ($C$) of a single electrode is calculated according to the following Eq. 1 [43,44]:

$$C = \frac{Q}{A\Delta U} \tag{1}$$

where $Q$ is the average charge, $A$ is the effective area referring to the geometric area of the electrochromic electrode, and $\Delta U$ is the voltage window (excluding the IR drop) [45]. Based on the GCD test, the value of $Q$ can be obtained by the following Eq. 2:

$$Q = \int_0^t i\mathrm{d}t = i\int_0^t \mathrm{d}t \tag{2}$$

The areal capacitance values of the $W_{18}O_{49}$/PANI film are 79.56, 79.09, 75.23, 72.66, and 71.02 mF/cm$^2$ at different current densities of 0.1, 0.2, 0.5, 0.8, 1 mA/cm$^2$, respectively (Fig. 2b), which is much larger than those of the other two films. The capacitance value of the $W_{18}O_{49}$/PANI film is much higher than the sum of individual $W_{18}O_{49}$ and PANI films (Fig. 2b), which can be mostly ascribed to the synergistic effect between PANI and $W_{18}O_{49}$, further strengthening the energy storage ability. The increase in areal capacitance may be due to the increase in surface roughness of the electrode, which could boost ion diffusion and charge transfer. By using the well-characterized mediator (potassium ferricyanide), the surface roughness factors (the ratio of an electrochemical active area over the geometric area) of pure $W_{18}O_{49}$, pure PANI and $W_{18}O_{49}$/PANI were calculated to be 0.52, 1.27, 1.22, respectively. The actual surface area of $W_{18}O_{49}$/PANI film is calculated according to the Randles-Sevcik equation [46,47]. The surface roughness factor of the $W_{18}O_{49}$/PANI film (1.22) is less than that of PANI (1.27), as well as the sum of individual $W_{18}O_{49}$ and PANI, while the capacitance value of the $W_{18}O_{49}$/PANI film is much higher than the sum of individual $W_{18}O_{49}$ and PANI films (Fig. 2b). Therefore, the remarkable areal capacitance improvement of the $W_{18}O_{49}$ for the hybrid film is mainly attributed to the synergistic effect between $W_{18}O_{49}$ and PANI, in other words, the formation of the donor (PANI)-acceptor ($W_{18}O_{49}$) pair.

Moreover, the similar pattern of the charging and discharging curves, combined with the areal charging and discharging capacities of 80.1 and 79.6 mF/cm$^2$ (Fig. S12c) reveal the good capacitive property [31] of $W_{18}O_{49}$/PANI. Afterward, we tested if a thicker PANI in $W_{18}O_{49}$/PANI brings a better capacitive behavior. When the deposition time continues to increase to 400 s, the areal capacitance is slightly lower, as shown in Fig. S12d (Supporting information), which may be due to the larger electrode impedance of $W_{18}O_{49}$/PANI (400 s) and is not conducive to improving the capacitive performance [21]. To further evaluate the electrochemical performance of the hybrid film, its stability is one of the most critical parameters. The CA measurements are carried out to study the stability of the films [9]. As shown in Fig. 2c, the hybrid film exhibits a slightly low current density than that of PANI film (Fig. S13b in Supporting information) at the beginning of the test, which is ascribed to the higher surface conductivity of the PANI film. On the other hand, the hybrid film affords much-enhanced stability than the PANI film after 3200 s cycling time, which could be ascribed to the strong contact between $W_{18}O_{49}$ and the FTO substrate. Moreover, the electrochemical stability is greatly enhanced after PANI is coated on the rough surface of $W_{18}O_{49}$. In contrast, as the PANI layer degrades in an acidic environment and loses most of its performance, the current density of PANI gradually decreases. Similarly, the original capacity of the hybrid film still maintains 80% after 100 cycles (Fig. 2d), which is superior to the performance of PANI films (Fig. S13c in Supporting information). This demonstrates the great capacitance reproducibility of the $W_{18}O_{49}$/PANI hybrid film, showing excellent application potential in electrochromic capacitors.

The $W_{18}O_{49}$/PANI film turns from dark blue to green, yellow, and light blue, during the potential range from 1.0 V to −0.6 V (Fig. 3a), indicating the large optical modulation range of the hybrid film. Compared with the PANI film (Fig. S14), the $W_{18}O_{49}$/PANI film displays richer colors, which is ascribed to the diverse absorption characteristics of the $W_{18}O_{49}$ and PANI at different voltages. The transmittance of $W_{18}O_{49}$/PANI film at 300∼1400 nm gradually increases when the applied voltage is from 1.0 V to −0.6 V (Fig. 3b), involving the process of $Cl^-$ extraction and $Al^{3+}$ intercalation [20,31]. The transmittance modulation ($\Delta T$) of the $W_{18}O_{49}$/PANI film is calculated to be 70.2% (652 nm), comparable to the PANI film (63.3%, Fig. S15a in Supporting information). Moreover, the $W_{18}O_{49}$/PANI film has a wider optical modulation range from 800∼1050 nm, which has excellently higher $\Delta T$ (∼44.2%) in comparison to the PANI film. The bleached/colored switching process of the $W_{18}O_{49}$/PANI film is determined by alternately applying a voltage at 1.0 V for 25 s followed by −0.6 V for 25 s on the film, whereas *in situ* monitoring is conducted of its transmittances at 652 nm. The dynamic switching of $W_{18}O_{49}$/PANI (Fig. 3c) for 400 s, in which the $W_{18}O_{49}$/PANI film exhibits $\Delta T$ of 64.2% at 652 nm is higher than that of the PANI film measured (53.0%, Fig. S15b in Supporting information), indicates that $W_{18}O_{49}$/PANI electrochromic film has good reversibility and cycling stability. Fig. 3d and Fig. S15c (Supporting information) show the reversible electrochromic switching behaviors of the $W_{18}O_{49}$/PANI and PANI films. Faster switching time in the bleached process (6.3 s) is achieved from the hybrid film, compared to the PANI film

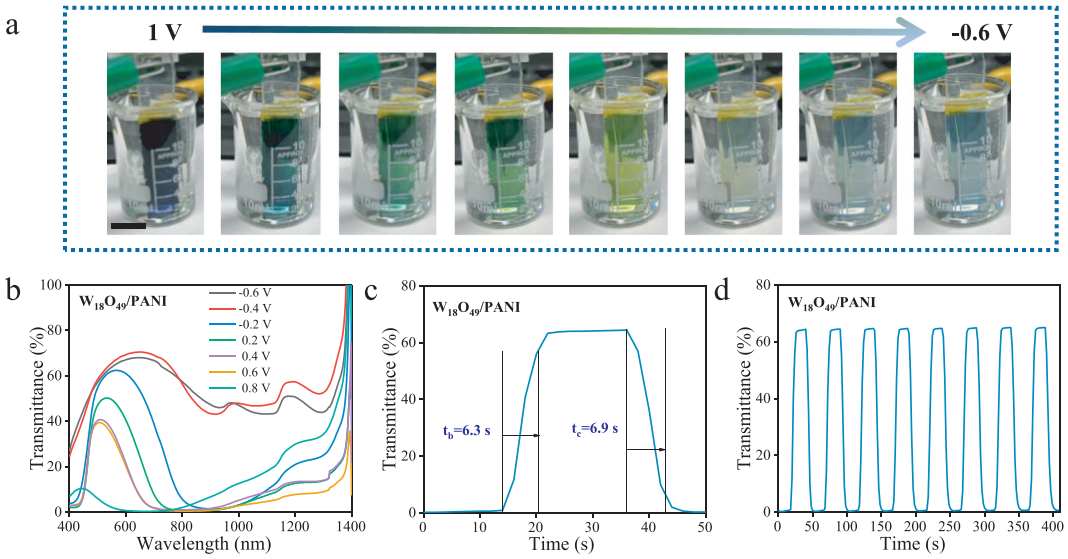


**Fig. 3.** (a) The photographs of the $W_{18}O_{49}$/PANI film ($1 \times 4.5$ cm$^2$) at different voltages, scale bar: 1 cm. (b) The transmittance spectra of the $W_{18}O_{49}$/PANI film under different voltages. (c) The dynamic test of the $W_{18}O_{49}$/PANI film at 652 nm in the potential window between −0.6 and 1.0 V for 400 s. (d) Transmittance at 652 nm *versus* time for electrochromic switching of $W_{18}O_{49}$/PANI film.

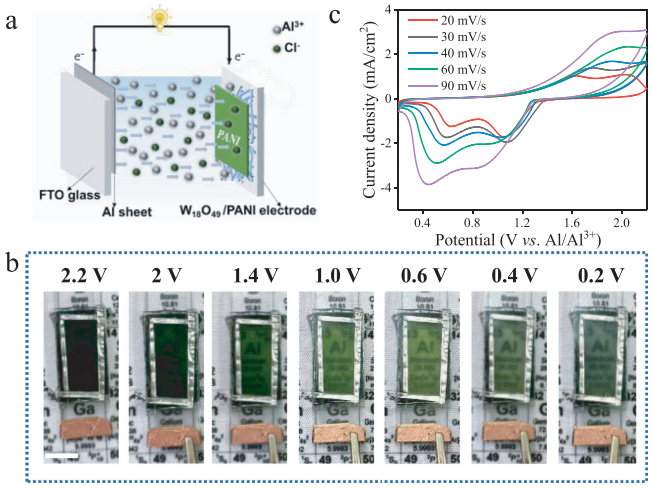


**Fig. 4.** (a) Schematic structure of the $W_{18}O_{49}$/PANI ECD. (b) The photographs of the $W_{18}O_{49}$/PANI ECD in different states under indicated potentials, scale bar: 1 cm. (c) The CV curves of the $W_{18}O_{49}$/PANI ECD between 0.2 V and 2.2 V.

(13.3 s), which is ascribed to the layer of $W_{18}O_{49}$ nanowires providing large porous space and thus making ion diffusion easier, as well as the synergistic effect of the $W_{18}O_{49}$/PANI. While the coloration time of PANI and $W_{18}O_{49}$/PANI films are 3.7 and 6.9 s, respectively. Because of the instability of PANI in the colored state, its colored time is slightly shorter than that of the hybrid film. Besides, the donor-acceptor pair between PANI and $W_{18}O_{49}$ can further enhance the electron transfer rate and has a positive effect on the ion diffusion efficiency and color switching speed of $W_{18}O_{49}$/PANI.

The schematic diagram of a prototype device demonstrates the potential of this novel $W_{18}O_{49}$/PANI ECD (Fig. 4a). Aluminum (Al) is chosen as the anode to construct the $W_{18}O_{49}$/PANI ECD, which has a strong reducing ability and easily loses electrons [22]. Fig. 4b shows the visually distinguished color change of the ECD, from light blue to light green, green, blue, and dark blue at the voltages from 0.2 V to 2.2 V, where a deeper color means a higher charging extent [22], indicating a function of the capacitive level-visualization of ECD-based energy storage device [21]. In addition, the optical transmission spectrum of the $W_{18}O_{49}$/PANI ECD under different applied voltages was also tested (Fig. S16 in Supporting information), which shows the good optical modulation ($\Delta T = 50.0\%$ at 532 nm) of the $W_{18}O_{49}$/PANI ECD. The CV curves of the device from 2.2 V to 0.2 V at different scan rates are presented in Fig. 4c, as the scan speed increases, the response current density of the $W_{18}O_{49}$/PANI ECD also increases, demonstrating the excellent kinetics and reversibility of the interfacial Faradaic redox reaction [21]. The CV curve potential window range of the ECD is enlarged due to the two electrodes system and the internal resistance of the device [6,22]. As depicted in Fig. S17a (Supporting information), the GCD curves of the device at different current densities under the voltage window of 2.2~0.2 V show nonlinear characteristics, which may be due to the redox reaction [21] of $W_{18}O_{49}$ or PANI. According to the Eqs. 1 and 2 described above, the areal capacitances of $W_{18}O_{49}$/PANI ECD are 46.15, 45.16, 43.78, 43.20, 42.83, and 42.36 mF/cm$^2$, respectively. The charge capacity of the $W_{18}O_{49}$/PANI ECD is far superior to that of the pure $W_{18}O_{49}$ ECD and PANI ECD (Fig. S17b in Supporting information), which shows that the hybrid film ECD has excellent application strength in energy storage.

Previous reports have demonstrated that Al with strong reducing power exhibits large negative potentials and can be used to establish a large potential gradient for the rapid discharge process using electrochromic electrodes [22,48]. Electron transfer can occur when $W_{18}O_{49}$/PANI film is connected to a metallic Al electrode due to the potential difference between $W_{18}O_{49}$/PANI with Al, which could produce a current that exhibits battery-like characteristics [15,42]. Meanwhile, the transferred electrons induce spontaneous discoloration of the $W_{18}O_{49}$/PANI, enabling the device to function without an external power supply. The color of the device changes from the initial dark green to light yellow and finally to light blue as shown in Fig. S18 (Supporting information), which reflects the energy-saving property of $W_{18}O_{49}$/PANI ECD. Afterward, the as-prepared $W_{18}O_{49}$/PANI ECD can be charged by an external bias, accompanied by the color recovery from light blue to dark blue; a deeper color means a higher charging degree. In this sense, the energy storage level of the $W_{18}O_{49}$/PANI ECD can be indicated through the color state.

To further demonstrate the battery function of the $W_{18}O_{49}$/PANI electrochromic device, Mg is selected to construct the battery in-

stead of Al to obtain a larger potential [49–52] output a red light-emitting diode LED (~1.8 V) can be lit up when the $W_{18}O_{49}$/PANI and Al electrodes are connected. The pictures of LED at different time are presented in Fig. S19a (Supporting information). Compared with the LED lightened by the PANI-Mg pair (Fig. S19b in Supporting information), it can be found that the energy delivered by the $W_{18}O_{49}$/PANI-Mg battery can continuously light up a red LED for more than 2 h. In contrast, the PANI-Mg system can only light up the LED for a short time, demonstrating excellent capacitance characteristics of the $W_{18}O_{49}$/PANI hybrid device.

In conclusion, the $W_{18}O_{49}$/PANI hybrid film-based multicolored ECD is successfully proposed. Because of the individual electrochromic characteristics of PANI and $W_{18}O_{49}$, the color of the hybrid film exhibits richer color than that of PANI. Due to the formation of the donor-acceptor system (PANI-$W_{18}O_{49}$) as well as the synergistic effect, the $W_{18}O_{49}$/PANI hybrid film exhibits excellent electrochemical stability, good optical modulation, high areal specific capacitance, and excellent capacitance retention, which shows a profound impact on the development of multifunctional ECDs and promises their potential applications in energy-efficient technologies.

## Declaration of competing interest

The authors declare that they have no known competing financial interests or personal relationships that could have appeared to influence the work reported in this paper.

## Acknowledgments

This work was supported by the National Natural Scientific Foundation of China (No. 21804074), China Postdoctoral Science Foundation (No. 2020T130331), and the Open Funds of the State Key Laboratory of Physical Chemistry of Solid Surfaces (No. 202023).

## Supplementary materials

Supplementary material associated with this article can be found, in the online version, at doi:10.1016/j.cclet.2023.108305.

## References

[1] P. Yang, P. Sun, W. Mai, Mater. Today 19 (2016) 394–402.
[2] Z. Tong, Y. Tian, H. Zhang, et al., Sci. China Chem. 60 (2017) 13–37.
[3] Y. Zhai, J. Li, S. Shen, et al., Adv. Funct. Mater. 32 (2022) 2109848.
[4] H. Li, L. McRae, C.J. Firby, et al., Adv. Mater. 31 (2019) 1807065.
[5] Z. Tong, R. Lian, R. Yang, et al., Energy Storage Mater. 44 (2022) 497–507.
[6] M.A. Farahmand Nejad, S. Ranjbar, C. Parolo, et al., Mater. Today 50 (2021) 476–498.
[7] Q. Huang, G. Dong, Y. Xiao, et al., Electrochim. Acta 252 (2017) 331–337.
[8] S.I. Park, Y.J. Quan, S.H. Kim, et al., Int. J. Precis Eng. Manuf.-Green Technol. 3 (2016) 397–421.
[9] T.V. Nguyen, H.H. Do, T.Q. Trung, et al., J. Alloys Compd. 882 (2021) 160718.
[10] G. Yang, Y.M. Zhang, Y. Cai, et al., Chem. Soc. Rev. 49 (2020) 8687–8720.
[11] K.W. Kim, J.K. Lee, X. Tang, et al., Dyes Pigm. 190 (2021) 109321.
[12] D.S. Dalavi, R.S. Desai, P.S. Patil, J. Mater. Chem. A 10 (2022) 1179–1226.
[13] Q. Huang, J. Wang, H. Gong, et al., J. Mater. Chem. A 9 (2021) 6451–6459.
[14] H. Li, C.J. Firby, A.Y. Elezzabi, Joule 3 (2019) 2268–2278.
[15] J. Zhao, Y. Tian, Z. Wang, et al., Angew. Chem. Int. Ed. 55 (2016) 7161–7165.
[16] S. Cong, Y. Tian, Q. Li, et al., Adv. Mater. 26 (2014) 4260–4267.
[17] J. Zhang, J.P. Tu, G.H. Du, et al., Sol. Energy Mater. Sol. Cells 114 (2013) 31.
[18] Y. Chen, Y. Wang, P. Sun, et al., J. Mater. Chem. A 3 (2015) 20614–20618.
[19] Z. Tong, N. Li, H. Lv, et al., Sol. Energy Mater. Sol. Cells 146 (2016) 135–143.
[20] Y. Wang, X. Zhong, X. Liu, et al., J. Mater. Chem. A 10 (2022) 3944–3952.
[21] Y. Zhong, Z. Chai, Z. Liang, et al., ACS Appl. Mater. Interfaces 9 (2017) 34085–34092.
[22] J. Wang, L. Zhang, L. Yu, et al., Nat. Commun. 5 (2014) 4921.
[23] G. Cai, J. Tu, D. Zhou, et al., J. Phys. Chem. C 117 (2013) 15967–15975.
[24] Y. Shi, Y. Zhang, K. Tang, et al., Chem. Eng. J. 355 (2019) 942–951.
[25] J.L. Wang, Y.R. Lu, H.H. Li, et al., J. Am. Chem. Soc. 139 (2017) 9921–9926.
[26] S. Xu, X. Li, Y. Ou, et al., Inorg. Chem. Front. 6 (2019) 680–686.
[27] X. Li, J. Chu, Y. Cheng, et al., Mater. Lett. 275 (2020) 128081.
[28] S.H. Patil, A.P. Gaikwad, S.D. Sathaye, et al., Electrochim. Acta 265 (2018) 556–568.
[29] Y. Yue, H. Li, K. Li, et al., J. Phys. Chem. Solids 110 (2017) 284–289.
[30] J. Pan, R. Zheng, Y. Wang, et al., Sol. Energy Mater. Sol. Cells 207 (2020) 110337.
[31] Y. Tian, S. Cong, W. Su, et al., Nano Lett. 14 (2014) 2150–2156.
[32] P. Yang, P. Sun, L. Du, et al., J. Phys. Chem. C 119 (2015) 16483–16489.
[33] P. Snauwaert, R. Lazzaroni, J. Riga, et al., Synth. Metals 18 (1987) 335–340.
[34] N.A. Kumar, H.J. Choi, Y.R. Shin, et al., ACS Nano 6 (2012) 1715–1723.
[35] H.S. Nalwa, Appl. Organomet. Chem. 5 (1991) 349–377.
[36] T. Kobayashi, H. Yoneyama, H. Tamura, J. Electroanal. Chem. 177 (1984) 293–297.
[37] A. Rudge, J. Davey, I. Raistrick, et al., J. Power Sources 47 (1994) 89–107.
[38] F. Fusalba, D. Bélanger, Electrochim. Acta 45 (2000) 3877–3883.
[39] Z. Wang, Q. Zhang, S. Cong, et al., Adv. Opt. Mater. 5 (2017) 1700194.
[40] K. Zhou, H. Wang, J. Jiu, et al., Chem. Eng. J. 345 (2018) 290–299.
[41] A.J. Heeger, J. Phys. Chem. B 105 (2001) 8475–8491.
[42] X. Chang, R. Hu, S. Sun, et al., Appl. Surf. Sci. 441 (2018) 105–112.
[43] W.W. Liu, Y.Q. Feng, X.B. Yan, et al., Adv. Funct. Mater. 23 (2013) 4111–4122.
[44] Y. Gogotsi, P. Simon, Science 334 (2011) 917–918.
[45] M. Liu, K. Zhang, M. Si, et al., Carbon 153 (2019) 707–716.
[46] N. Wu, L. Jiao, S. Song, et al., Anal. Chem. 93 (2021) 15982–15989.
[47] D. Voiry, M. Chhowalla, Y. Gogotsi, et al., ACS Nano 12 (2018) 9635–9638.
[48] Y. Luo, H. Jin, Y. Lu, et al., ACS Energy Lett. 7 (2022) 1880–1887.
[49] H. Zhang, Y. Yu, L. Zhang, et al., Chem. Sci. 7 (2016) 6721–6727.
[50] Y. Zhai, Y. Li, H. Zhang, et al., ACS Appl. Mater. Interfaces 11 (2019) 28072–28077.
[51] J. Sun, Y. Li, J. Sun, et al., Chem. Commun. 55 (2019) 12060–12063.
[52] Q. Ma, H. Zhang, J. Chen, et al., ACS Central Sci. 6 (2020) 2209–2216.